Structures, Vibrations, and Force Fields of Dithiophosphate Wear Inhibitors from *ab Initio* Quantum Chemistry

Shaoyi Jiang,[†] Siddharth Dasgupta,[†] Mario Blanco,[†] Rawls Frazier,[‡] Elaine S. Yamaguchi,[§] Yongchun Tang,[||] and William A. Goddard, III*,[†]

Materials and Process Simulation Center (CN 1411), Beckman Institute (139-74), Division of Chemistry and Chemical Engineering, California Institute of Technology, Pasadena, California 91125, Chevron Research and Technology Company, 100 Chevron Way, Richmond, California 94802, Chevron Chemical Company, Oronite Technology Group, 100 Chevron Way, Richmond, California 94802, and Chevron Petroleum Technology Company, 1300 Beach Boulevard, La Habra, California 90631

Received: February 29, 1996; In Final Form: June 28, 1996[⊗]

Zinc dithiophosphates (ZnDTPs) are ubiquitous lubricating oil additives in today's passenger car motor oils, providing the important functions of wear and oxidation inhibition. However, the molecular-level mechanism by which these materials reduce wear is not understood. As a first step in developing an understanding of this mechanism, we used *ab initio* quantum chemical methods to examine the structures, vibrations, and energetics of these systems. The results show that the two phosphorus−sulfur bonds of the dithiophosphate of ZnDTPs are *equivalent* and have character intermediate between single and double bonds. This contrasts with the paradigm of one double bond (P═S) and one single bond (P−S) often used. Vibrational studies of DTP systems lead to a strong IR transition at about 650 cm^{-1} and a weak transition at about 530 cm^{-1}. We find modes in good agreement with experiment, where the high-frequency mode is *antisymmetric PS stretch* (not P═S), while the lower mode is *symmetric PS stretch* (not P−S). On the basis of the *ab initio* calculation results, we used the biased Hessian method to develop a vibrationally accurate force field (FF) for ZnDTPs. This FF can be used to examine the binding of DTPs to metal and metal oxide surfaces.

I. Introduction

Valve train wear of internal combustion engines is greatly reduced by adding zinc dithiophosphate (ZnDTP) wear inhibitors,

$$Zn[(RO)_2PS_2]_2$$

to lubricating oil.[1−3] In particular the ZnDTPs derived from secondary alcohols (termed secondary alkyl) provide excellent valve train wear control in comparison to ZnDTPs derived from primary alcohols or phenols.[1] Although ZnDTPs have proved quite effective as wear inhibitors and have been in use for nearly 50 years, there is little molecular-level understanding of how they work.[4]

Understanding the mechanism of action of ZnDTPs could reveal insights to developing more effective ones. This is important for three reasons.

(i) The proposed GF-2 specifications set a new, upper limit to phosphorus concentrations in passenger car motor oil that challenge current wear performance.[5] Specifically, the International Lubricant Standardization and Approval Committee (ILSAC) GF-2 requirements for passenger car motor oils will lower phosphorus limits from the maximum of 0.12% allowed by ILSAC GF-1 to a maximum of 0.10%. This requirement removes ≈17% of the ZnDTP from the formulation. Thus, more effective ZnDTPs or other additives are needed to make up for the loss of wear protection.[6]

(ii) Secondly, phosphorus (derived from the ZnDTP) has a deleterious effect on emissions control catalytic converters.[7] This puts additional downward pressure on the overall concentration of ZnDTP in the oil.

(iii) Finally, there are environmental concerns associated with the usage of ZnDTPs.[8]

It is often assumed[9,10] that one phosphorus−sulfur bond of the dithiophosphate of ZnDTPs has double-bond character (P═S), while the other has single-bond character (P−S) and is bonded to the Zn. Vibrational studies of DTP systems lead to a strong IR transition at about 650 cm^{-1} that is assigned as P═S and a weaker transition at about 530 cm^{-1} that is assigned as P−S.[10] However other studies have assumed equivalent bonds (based on NMR evidence).[11]

In this work we use *ab initio* quantum chemical (QC) methods to determine structural, vibrational, and energetic characteristics of ZnDTP molecules. On the basis of these *ab initio* results, we developed an accurate force field (FF) for use in studying the binding of DTPs to metal and metal oxide surfaces.

Section II describes details for the QC and FF calculations. Section III reports the structures, vibrations, and energetics for various species, concluding with the properties of $Zn(DTP)_2$ monomer and $Zn_2(DTP)_4$ dimer. The results are summarized in section IV.

II. Calculational Details

II.A. Quantum Chemistry. Unless stated otherwise, all calculations were carried out with the PS-GVB program[12,13] at the Hartree−Fock (HF) level using the LAV3P*** basis set. The LAV3P basis set[13] uses the Hay and Wadt effective core potentials (ECP)[14] for the atoms Na−La and Hf−Bi and an all-electron 6-31G basis description for atoms H−Ne.[15] This basis set differs from the standard double-ζ contraction (LANL1DZ) of the Hay and Wadt basis set[14] in that the three s basis functions are left uncontracted (the remainder of the basis uses the standard double-ζ contraction). The notation *** indicates that

* To whom correspondence should be addressed.
[†] California Institute of Technology.
[‡] Chevron Research and Technology Co.
[§] Chevron Chemical Co.
[||] Chevron Petroleum Technology Co.
[⊗] Abstract published in *Advance ACS Abstracts,* August 15, 1996.

S0022-3654(96)00649-1 CCC: $12.00

d polarization functions (exponent = 0.1202) are added for Zn, d polarization functions (exponents of 0.80, 0.80, 0.3934, 0.487) are added for (C, O, P, S, respectively), and p polarization functions (exponent = 1.10) are added for H. The notation **** indicates that additional f polarization functions (exponent = 1.81) are included on the zinc atom.

As discussed in section III some calculations were carried out using other descriptions.

The all-electron MSV basis set of Rappé and Goddard[13,16] is a 4-21G basis optimized for all atoms through Xe. Here *** indicates the use of polarization functions.

We also considered LANL1DZ, the standard double-ζ contraction of the ECP basis from Hay and Wadt (the default in Gaussian 92[17]) with the all-electron 6-31G description for H−Ne. This does not include polarization functions.

We also considered the DOLG*** basis set[18] (a triple-ζ contraction of an optimized (8s7p6d)/[6s5p3d] basis) with the *ab initio* ECP (pseudopotential) replacing only the 1s, 2s, and 2p core electrons but not 3s and 3p.

In addition, for some systems we included electron correlation effects. Thus we used (1) local Moller−Plesset second-order perturbation theory (MP2)[13] with He/Ne frozen core, (2) generalized valence bond (GVB) theory[13] with Zn−S as GVB pairs, and (3) density functional theory (DFT)[13] with the Becke gradient correction and the Lee−Yang−Parr correlation functional.

Molecular charges are based on the electrostatic field[13,19] from *ab initio* HF calculations. In this procedure, the electrostatic field at a grid of points is calculated from the HF wave function. Using the grid points outside of the van der Waals (vdw) radii, atom-centered charges are derived so as to match the HF potential while reproducing the dipole moment from HF.[12]

II.B. Force Fields and Charges. The universal force field (UFF)[20b] was modified to fit the *ab initio* calculations using biased Hessian techniques.[21] Here we write the total potential energy of a molecule as a superposition of short-range valence (E_{val}) and long-range nonbonded (E_{nb}) interactions,

$$E = E_{val} + E_{nb} \tag{1}$$

where the valence interactions consist of bond stretch (E_{bond}), bond-angle bend (E_{angle}), dihedral angle torsion ($E_{torsion}$), and inversion ($E_{inversion}$) terms,

$$E_{val} = E_{bond} + E_{angle} + E_{torsion} + E_{inversion} \tag{2}$$

while the nonbonded interactions consist of vdw (E_{vdw}) and electrostatic (E_Q) terms

$$E_{nb} = E_{vdw} + E_Q \tag{3}$$

In this work E_{bond}, E_{angle}, $E_{torsion}$, E_{vdw}, and E_Q are described by harmonic, cosine harmonic (cosine-stretch for the S−P−S term), torsion Fourier, exponential-6, and Coulomb functions, respectively:[20]

$$E_{bond} = \frac{1}{2}K_b(R - R_0)^2 \tag{4}$$

$$E_{angle} = \frac{1}{2}\frac{K_\theta}{(\sin\theta_0)^2}(\cos\theta - \cos\theta_0)^2 \tag{5a}$$

$$E_{angle(SPS)} = \frac{1}{2}\frac{K_\theta}{(\sin\theta_0)^2}(\cos\theta - \cos\theta_0)^2 + K_{RR}(R_1 - R_{10})(R_2 - R_{20}) \tag{5b}$$

$$E_{torsion} = \sum_{m=0}^{3} V_m \cos m\phi \tag{6}$$

$$E_{vdw} = D_v\left\{\left[\left(\frac{6}{\zeta - 6}\right)e^{\zeta(1-R/R_v)}\right] - \left[\left(\frac{\zeta}{\zeta - 6}\right)\left(\frac{R}{R_v}\right)^6\right]\right\} \tag{7}$$

$$E_Q = \sum_{i>j}\frac{Q_iQ_j}{\epsilon_0 R_{ij}} \tag{8}$$

(where $1/\epsilon_0 = 332.0637$ if E is in kcal/mol, R is in angstroms, and charges are in electron units).

Using the biased Hessian method,[21,22] the equilibrium bond lengths (R_0) and angles (θ_0) were determined to fit the QC geometries, and the force constants (K_b, K_θ, and K_{RR}) were determined to fit the QC vibrational frequencies. The torsional barriers (V_m) were adjusted to reproduce the conformational energy differences from HF calculations. Nonbond interactions (vdw and Q) are not used between nearest neighbors (1−2 interactions) and next nearest neighbors (1−3 interactions). The dielectric constant is taken as $\epsilon_0 = 1$, and nonbond cutoffs were eschewed.

The purpose in developing the FF is to predict accurate structural, vibrational, and energetic properties of large molecules. Thus, it is essential to have a general approach that can provide charges for the systems. We used the charge equilibration (QEq) method[23] but readjusted the QEq electronegativities to reproduce the charges from quantum calculations on the model systems. This is denoted as QEq*. We required that $Q_{Zn} = +2$ and $Q_{DTP} = -1$. This allows dissociative processes of the Zn cluster and binding to an Fe_2O_3 surface to be described with the same charges.

The Zn−S interaction was treated as nonbonding so that dissociation of DTP from the Zn could be described. Charges were determined with QEq*, as discussed above. The Zn−S interaction was taken to be a Morse function,

$$E_{vdw(Zn-S)} = D_v[\chi^2 - 2\chi] \tag{9}$$

where

$$\chi = \exp\left[-\frac{\zeta}{2}\left(\frac{R}{R_v} - 1\right)\right] \tag{10}$$

We used a Morse function [rather than (7)] because it mimics the bonding from a partially covalent bond. The equilibrium position (R_v) was determined to fit the *ab initio* interatomic distance from QC calculations of $Zn(DTP)_2$. The dissociation energy (D_v) was determined to fit the snap binding energy.[24] The ζ was chosen to reproduce the vibrational frequency.

The nonbonded S−S interaction was taken to be pure repulsive exponential,

$$E_{vdw(S-S)} = D_v\, e^{\zeta(1-R/R_v)} \tag{11}$$

where R_v and D_v were adjusted to reproduce the *ab initio* structures of the $Zn_2(DTP)_4$ dimer.

This FF is denoted as MSX (materials simulation with limited cross terms).

II.C. Vibrations. Vibrational frequencies were obtained by diagonalizing the full second-derivative matrix (Hessian) evaluated at the optimum HF structure using HF/LAV3P***. The infrared intensities were also computed from coupled perturbed Hartree−Fock (CPHF) calculations of the derivative of the dipole moment with respect to changes in the nuclear coordinates.

III. Results and Discussion

Because it is the smallest alkyl dithiophosphate, we used dimethyl DTP as the model compound for studying structures and extracting scaling parameters from experiment and HF theory.

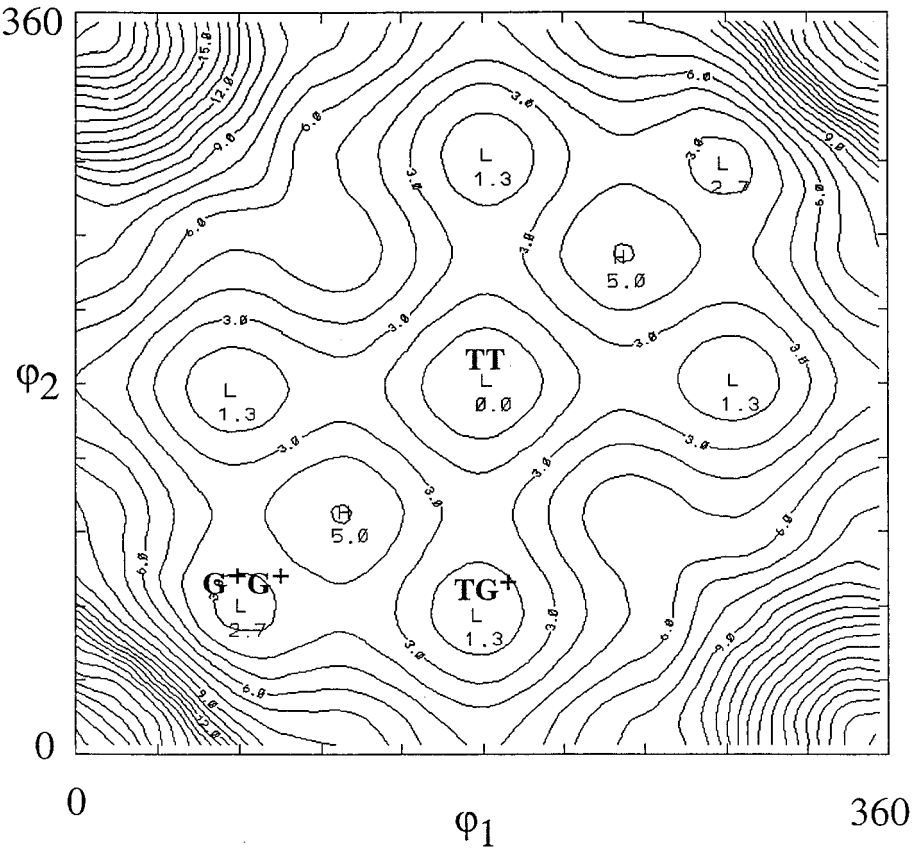

Figure 1. Potential energy surface for dimethyl DTP anion $[(MeO)_2PS_2]^-$ using the UFF force field (the parameters of the UFF force field were preliminarily modified to reproduce *ab initio* results and were later fine-tuned to form the MSX force field). For each H_3CO-PO dihedral (ϕ_1 and ϕ_2) all other geometric quantities were optimized. Contours are at 1 kcal/mol intervals. All maxima (H) and minima (L) are listed with their energies. TT, TG, and GG indicate trans−trans, trans−gauche, and gauche$^+$−gauche$^+$ conformers.

III.A. DTP Anion. *III.A.a. Conformations.*

There are several low-energy conformations of the alkoxy groups for

$DTP^- = (MeO)_2PS_2^-$ =

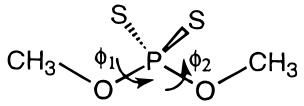

To determine the most important conformations, we first used the UFF[20b] to calculate the optimum structural parameters as a function of torsional angles, ϕ_1 and ϕ_2, about the two P−O bonds. The contour plots of this potential surface are shown in Figure 1, which has three types of minima corresponding to (see Figure 2) (i) one *tt* conformer ($\phi_1 = \phi_2 = 180°$), the minimum energy; (ii) four *tg*-like conformers ($\phi_1 = 180°$ and $\phi_2 = 66°$) at 1.3 kcal/mol; and (iii) two g^+g^+-like conformers ($\phi_1 = 66°$ and $\phi_2 = 66°$) at 2.7 kcal/mol. A minimum might have been anticipated for g^+g^-; however, bad steric interactions prevent a local minimum.

We carried out QC calculations to optimize the three conformers (*tt*, tg^+, and g^+g^+) at the HF/LAV3P*** level. The HF geometries are shown in Figure 2, with key quantities tabulated in Table 1S (supporting information). From HF, the most stable conformation of the isolated dimethyl DTP anion is *tt*, followed by *tg* at 0.17 kcal/mol and g^+g^+ at 0.62 kcal/mol. We find that the two P−S bonds of DTP^- are equivalent, which is consistent with experiment.[25−28] The P−S bond lengths vary from 1.993 to 1.983 Å for these conformers, as shown in Figure 2.

III.A.b. Vibrations. For the three stable conformations, we calculated the vibrational frequencies. The calculated vibrational frequencies and infrared intensities of the two modes involving phosphorus−sulfur stretch character are shown in Figure 3 and tabulated in Table 1. The intense high-frequency mode (∼716 cm^{-1}) is antisymmetric stretch (PS_{anti}), while the weak lower mode (∼532 cm^{-1}) is symmetric stretch (PS_{sym}). Table 1 shows that the frequencies of these two modes depend strongly on conformation, differing by nearly 40 cm^{-1} between the *tt* and g^+g^+ conformers. It also shows that intensities are very sensitive to conformation. The intensity ratios $I(PS_{anti})/I(PS_{sym})$ are predicted to be between 54 and 145 for these conformers.

III.A.c. MSX Force Field. The charges are obtained from the QEq method,[23] the parameters (electronegativities) of which were adjusted to reproduce the QC charges. The comparison in Table 2 shows that these QEq* charges fit the QC quite well.

The FF parameters were optimized as follows. The equilibrium bond lengths and angles in the FF were first fit to the QC geometries. The force constants were then fit to the QC vibrational frequencies by the biased Hessian method.[21] Finally, the torsional barriers were adjusted to reproduce the energy differences between different conformers from the QC calculations. The parameters for this MSX FF are given in Tables 3 and 4. Tables 1S and 1 show that the geometries and vibrational frequencies from this FF are in excellent agreement with QC results.

III.B. Zn(SH)DTP. *III.B.a. Binding to the Zn.* The model compound $Zn(SH)[(CH_3O)_2PS_2]$ was used to determine the preferred coordination of Zn with DTP. We considered three possible Zn coordinations: (i) two sulfur atoms (labeled SS); (ii) two oxygen atoms (OO); or (iii) one sulfur and one oxygen atom (SO). QC calculations (both all-electron and ECP) were carried out on the *tt* conformation for each case. The best calculations (*** with polarization functions added to all atoms) lead to the following (Table 2S, supporting information): SS (0.0), OS (10.5), and OO (28.0) from MSV*** (all electron);

TABLE 1: Vibrational Frequencies[a] and IR Intensities of the PS Stretch Modes for $(MeO)_2PS_2^-$

	tt			*tg*$^+$			*g*$^+$*g*$^+$		
	QC[b]	MSX	UFF	QC[a]	MSX	UFF	QC[a]	MSX	UFF
PS_{anti} ν(cm^{-1})	716	716	732	735	731	759	747	737	773
I(km/mol)	183.9			153.9			144.5		
PS_{sym} ν(cm^{-1})	532	533	522	547	546	553	576	572	674
I(km/mol)	3.4			2.0			1.0		
ratio I_{anti}/I_{sym}	54			77			145		

[a] Since an ECP is used, both PS-GVB and Gaussian 92 use numerical differences of the analytic gradient of the energy with respect to coordinates to calculate the Hessian for the vibrational frequencies. We used PS-GVB for all results quoted since it led to higher accuracy. For PS-GVB we find that using geometry changes of $\delta = 0.05$ Å gives accurate vibrational frequencies (all positive), while $\delta = 0.01$ and $\delta = 0.1$ both lead to some negative vibrational frequencies (−165 and −124 for $\delta = 0.01$ and −19 and −15 for $\delta = 0.1$). Gaussian 92 led to 16 negative vibrational frequencies at the optimum geometry. [b] HF/LAV3P***.

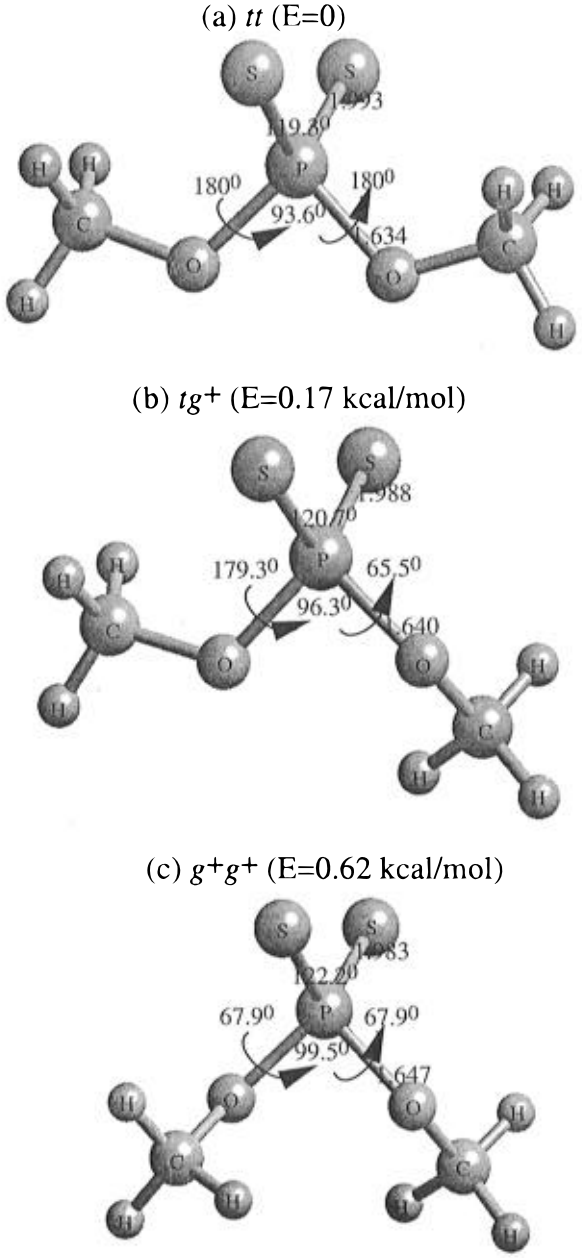

Figure 2. Conformers of $[(MeO)_2PS_2]^-$ from HF/LAV3P*** calculations. See Table 1S (supporting information) for details.

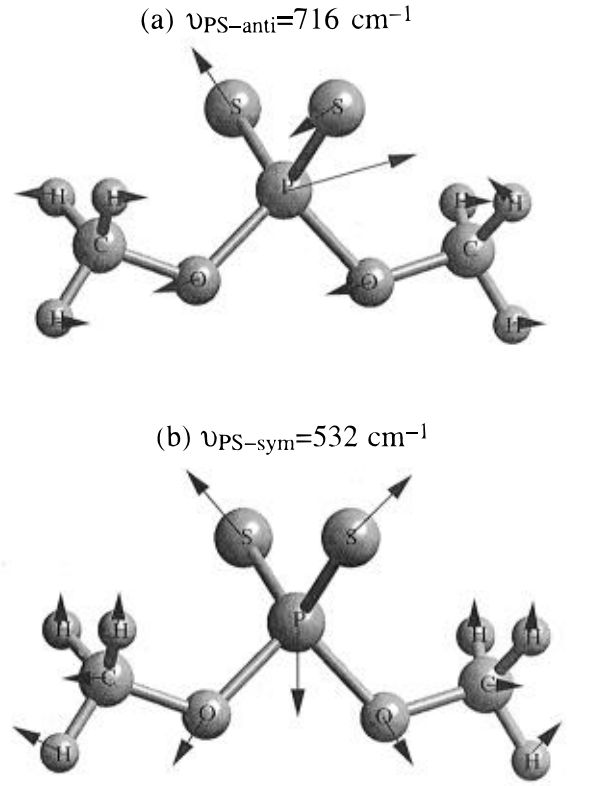

Figure 3. Vibrational modes of the *tt* conformation for $[(MeO)_2PS_2]^-$ from HF/LAV3P*** calculations: (a) PS antisymmetric stretch (PS_{anti}); (b) PS symmetric stretch (PS_{sym}).

TABLE 2: Charges for $(MeO)_2PS_2^-$ from QC and QEq*

	tt		*tg*$^+$		*g*$^+$*g*$^+$	
	QC[a]	QEq*[b]	QC[a]	QEq*[b]	QC[a]	QEq*[b]
S	−0.60	−0.60	−0.60	−0.62	−0.60	−0.57
P	0.47	0.46	0.49	0.47	0.53	0.48
O	−0.33	−0.33	−0.33	−0.34	−0.37	−0.35
C	0.13	0.13	0.12	0.13	0.17	0.13
H	0.04	0.04	0.04	0.06	0.02	0.02

[a] Electrostatic potential derived charges from HF/LAV3P*** calculations. [b] QEq* denotes QEq[23] but with the electronegativities modified as follows: $\chi_P = 5.463$, $\chi_S = 7.728$, $\chi_O = 7.801$, $\chi_C = 4.703$, and $\chi_H = 4.328$.

SS (0.0), OS (9.7), and OO (27.5) from LAV3P*** (ECP), where the numbers are relative energies in kcal/mol. Thus the SS coordination is lowest in energy, in accord with experimental observations.[25−28] The results in Table 2S show that the polarization functions are important in predicting the relative energies, and we focus on only such calculations in the remaining text.

III.B.b. Conformation of the Alkoxy Groups. We used HF/LAV3P*** to calculate the geometries [Figure 1S and Table 2S (supporting information)] of the three SS conformers of Zn(SH)$[(MeO)_2PS_2]$. As with the DTP anion, the *tt* and *tg*$^+$ conformers have essentially the same energies, but now *tt* is higher than *tg*$^+$ by 0.13 kcal/mol while *g*$^+$*g*$^+$ is at 1.19 kcal/mol. Bonding DTP to the Zn decreases the S−P−S angles of DTP anion by 10°, increases the S−P bonds by 0.035 Å, and decreases the P−O bonds by 0.047 Å. The two P−S bonds for Zn(SH)$[(MeO)_2PS_2]$ are equivalent. They vary from 2.033

TABLE 3: Valence Parameters of the MSX FF

bond (eq 4)	K_b [(kcal/mol)/Å^2]	R_0 (Å)
C−H	822.0	1.084
O−C	900.5	1.400
P−O	830.0	1.637
S−P	517.2	1.996

angle (eq 5)	K_a [(kcal/mol)/radian^2]	θ_0 (deg)	K_{R1R2} [(kcal/mol)/Å^2]
H−C−H	90.6	109.5	
O−C−H	136.7	109.4	
P−O−C	159.8	119.9	
O−P−O	154.4	92.2	
S−P−O	160.2	109.8	
S−P−S	164.3	121.0	80.3

torsion[a] (eq 6)	V_0	V_1	V_2	V_3
X−O−C−X	0.3	0.0	0.0	0.3
X−P−O−X	2.5	0.0	−5.2	2.5

[a] Units in kcal/mol.

TABLE 4: van der Waals Parameters of the MSX FF

	type[b]	R_v (Å)	D_v (kcal/mol)	ζ
		Diagonal[a]		
H	exp-6	3.195	0.015	12.38
C	exp-6	3.898	0.095	14.03
O	exp-6	3.405	0.096	13.48
P	exp-6	4.150	0.320	12.00
S	exp-6	4.030	0.344	12.00
Zn	exp-6	4.540	0.055	12.00
		Off-Diagonal		
S−S	pure-exp	5.8	0.205	9.8
Zn−S	Morse	2.448	31.8	12.0

[a] Diagonal parameters are from Dreiding.[20a] [b] See eqs 7, 9, and 11.

to 2.022 Å for these conformers, 0.04 Å longer than those of their anion counterparts.

III.C. Zn(DTP)$_2$, the Monomer. *III.C.a. Structure*. For the Zn(DTP)$_2$ monomer, we find that the optimum structure has the zinc atom coordinated with the four S of the two DTP anions in a distorted tetrahedral geometry (D_{2d} symmetry). Since the *tt* and *tg*$^+$ conformers of the DTP anions have essentially the same energies, we expect three low-energy conformers of the monomer. Indeed as shown in Table 5, the QC energies are within 0.14 kcal/mol (from HF/LAV3P*** calculations). The *ab initio* structure of Zn(DTP)-*tt* is shown in Figure 4, with key quantities tabulated in Table 5.

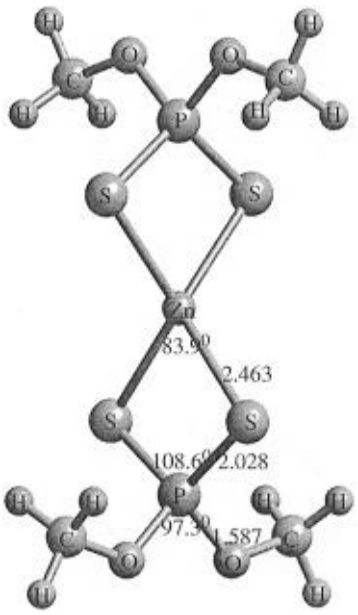

Figure 4. Optimum structure of the Zn[(MeO)$_2$PS$_2$]$_2$−*tt* monomer (from HF LAV3P*** calculations).

Most interesting here is that the four phosphorus−sulfur bonds are *equivalent* for all cases. Three conformers given in Table 5 lead to bond differences within 0.007 Å. This contrasts with the discussions in the literature[9,10] that assume that each DTP leads to one bond with double-bond character, P═S, and another with single-bond character, P−S. The calculated phosphorus−sulfur bond lengths are 2.028 Å, compared with the hypothetical lengths of a single (2.14 Å) and a double (1.94 Å) phosphorus−sulfur bond.[29] This indicates that the phosphorus−sulfur bonds of DTP have bond order $\sim 1^1/_2$.

III.C.b. Vibrations. We calculated vibrational frequencies of the Zn[(MeO)$_2$PS$_2$]$_2$ monomer at the HF/LAV3P*** level, leading to the phosphorus−sulfur stretch modes in Figures 5 and 6 for PS$_{anti}$ and PS$_{sym}$, respectively (see also Table 6).

TABLE 5: Calculated Structure of the Zn[(MeO)$_2$PS$_2$]$_2$ Monomer

	tt + *tt*			*tt* + *tg*$^+$			*tg*$^+$ + *tg*$^+$		
	QC[a]	MSX	UFF	QC[a]	MSX	UFF	QC[a]	MSX	UFF
				Bonds (Å)					
C−H	1.081	1.084	1.113	1.081	1.084	1.112	1.081	1.084	1.114
S−P	2.028	1.986	2.157	2.025	1.985	2.157	2.032	1.985	2.154
O−C	1.422	1.405	1.403	1.423	1.405	1.404	1.423	1.406	1.406
P−O	1.587	1.632	1.747	1.590	1.635	1.746	1.592	1.637	1.740
Zn−S	2.463[c]	2.389[c]	2.549	2.463	2.393	2.526	2.477	2.395	2.154
				Angles (deg)					
H−C−H	110.0	109.1	108.7	110.0	109.1	108.6	110.1	109.1	108.6
P−O−C	123.2	118.4	110.7	123.0	119.5	107.2	123.0	121.3	108.6
S−P−O	112.7	112.5	112.3	112.1	112.8	111.8	111.5	113.0	110.8
O−C−H	108.9	109.9	110.2	108.9	109.9	110.3	108.9	109.9	110.3
O−P−O	97.3	98.5	105.6	99.1	98.2	107.1	100.8	98.2	109.3
S−P−S	108.6	108.2	102.3	109.3	108.0	102.7	109.8	108.0	104.0
S−Zn−S	83.9	84.2	82.6	84.2	84.5	82.9	84.2	84.5	82.9
				Dihedrals (deg)					
C−O−P−O	180/180	180/180	180/180	179.7/−179.8	179.0/178.3	180/105.7	−179.3/60.8	179.7/51.5	177.8/70.1
C−O−P−O	180/180	180/180	180/180	−179.7/60.7	178.7/50.4	178/77.7	−179.3/60.8	179.0/51.5	177.8/70.1
				Energy (kcal/mol)					
	0.0[b]	0.0	0.0	−0.03	−0.2	−5.1	−0.14	−0.29	−7.0

[a] HF/LAV3P***. [b] Total energy: −574.034 14 hartrees. [c] The MSX FF was adjusted to reproduce the Zn−S bond distance expected from the best calculation [estimated to be 2.392A(MP2MSV****) = 2.463(HF/LAV3P***) − 0.071; see section III.D.b] rather than that of the HF/LAV3P*** level used for QC.

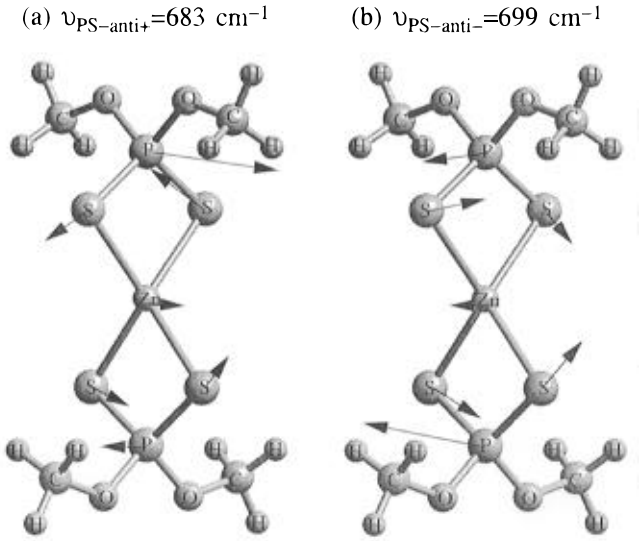

Figure 5. PS_{anti} vibrational modes of $Zn(DTP)_2$ monomer.

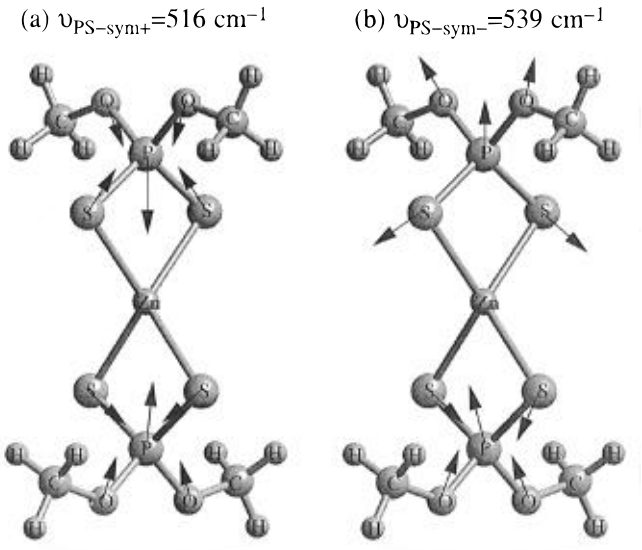

Figure 6. PS_{sym} vibrational modes of $Zn(DTP)_2$ monomer.

TABLE 6: Comparison of Experimental and QC Vibrational Frequencies (cm^{-1}) and IR Intensities[a] (km/mol) in the $Zn[(RO)_2PS_2]_2$ Monomer

R	source	PS_{anti}	PS_{sym}
Et	expt[10a]	655, 640	540, 526
	expt[30]	655s, 640s	542m, 525m
iPr	expt[10a]	649, 633	545, 530
	expt[30]	652s[c]	535s[c]
Me	QC[b]	699(105.5), 683(114.2)	539(7.1), 516(5.8)
scaling factor[d]	expt/QC	0.937	1.010

[a] m = medium; s = strong. QC intensities in parentheses. [b] HF/LAV3P***. [c] Only one mode was found. [d] Based on experimental data for R = ethyl.

Experimental studies of DTP systems generally lead to a strong IR transition at about 650 cm^{-1} and a weaker transition at about 540 cm^{-1}. Based on the P═S and P−S paradigm, these have been often assigned[10] as P═S and P−S, respectively. We find modes in good agreement with experiment, but the high-frequency mode is *antisymmetric stretch* (PS_{anti}, not P═S), while the lower mode is *symmetric stretch* (PS_{sym}, not P−S). Others[25,30] have assumed antisymmetric and symmetric stretch modes.

For $Zn(DTP)_2$ our calculations show that the two PS_{anti} modes are coupled via the zinc to form modes at 699 and 683 cm^{-1}. This corresponds to an average $\nu_{PS\text{-}anti}$ = 691 cm^{-1} with a splitting of 16, which compares well with experiment[10] [average of 647 cm^{-1} with a splitting of 15 (for R = Et)]. This interpretation of Zn-induced splitting contrasts with the previous interpretation which assumed the splittings to arise from different conformational isomers.[10]

TABLE 7: Averaged Vibrational Frequencies (cm^{-1}) for the Phosphorus−Sulfur Bond Stretch Modes of Various $Zn[(RO)_2PS_2]_2$ Monomers

	R			
	Me	iBu	iPr	phenyl
PS_{anti}				
MSX	647	647	654	650
QC[a]	647[a]			
Exp[b]		651[10b]	641[10a]	
		649[10e]	644[10b]	
		661[25]	643[10e]	
			652[30]	
PS_{sym}				
MSX	553	547	542	583
QC[a]	533[a]			
expt		552[10b]	538[10a]	
		550[10e]	532[10b]	
		554[25]	537[10e]	
			535[30]	

[a] Scaling factors of 0.937 for PS_{anti} and 1.01 for PS_{sym} were used.

Similarly the two PS_{sym} modes are calculated (QC) at an average $\nu_{PS\text{-}sym}$ = 527 cm^{-1} with a splitting of 23, which compares well with the experimental average of 533 cm^{-1} with a splitting of 14 (R = Et).

The theoretical values (for R = Me) compared to experiment (for R = Et) are 7% high for PS_{anti} and 1% low for PS_{sym}, but the Zn splittings are essentially the same (see Table 6).

For $Zn[(MeO)_2PS_2]_2$ the intensity ratio $I(PS_{anti})/I(PS_{sym})$ is predicted to be 17. Experiment also finds PS_{anti} to be stronger than PS_{sym}. In one experiment[25] the PS_{anti} absorption is described as considerably more intense than the PS_{sym} absorption, while in another[10e] the ratio is shown to be 3 to 1.

III.C.c. MSX FF. We developed the MSX FF to describe the $Zn[(MeO)_2PS_2]_2$ monomer. The FF is the same as in Tables 3 and 4 for $[(MeO)_2PS_2]^-$ except for additional terms to describe interactions between zinc and sulfur atoms, as discussed in section II. The MSX FF describes the zinc−sulfur interactions using the off-diagonal nonbonded Morse potential (9), with net charges of Q_{Zn} = +2.0 and Q_{DTP} = −1. The FF parameters were adjusted to reproduce the *ab initio* bond length [estimated to be 2.392A(MP2/MSV****) = 2.463(HF/LAV3P***) − 0.071; see section III.D.b], the snap bond energy (143.8 kcal/mol per bond), and the *ab initio* vibrational frequencies (scaled as in Table 6). The MSX FF describes well the *ab initio* structure of the monomer (see Table 5) and the scaled QC vibrations (see Table 7): $\nu_{PS\text{-}anti}$ = 647 cm^{-1} (647 from QC) and $\nu_{PS\text{-}sym}$ = 553 cm^{-1} (533 from QC).

We used the MSX FF to predict vibrational frequencies of diisobutyl (primary alkyl), diisopropyl (secondary alkyl), and diphenyl (aryl) $Zn(DTP)_2$ monomers. The results (Table 7) are in good agreement with experiment. (For R = iPr the MSX results are high by 11 cm^{-1} for PS_{anti} and by 6 cm^{-1} for PS_{sym}. For R = iBu the MSX results are low by 3 cm^{-1} for PS_{anti} and by 5 cm^{-1} for PS_{sym}.)

One goal of these studies is to obtain diagnostics for determining the changes in the Zn−DTP components when on real surfaces in real engines. Thus we are interested in modes that change significantly as the environment is changed (i.e. surface effects). It is of interest here that the weaker PS_{sym} mode changes by +41 cm^{-1} as iPr is replaced by phenyl, whereas the PS_{anti} mode changes by only −4 cm^{-1}.

TABLE 8: Snap Bond Energies[24] and Vibrational Frequencies for the Zn−DTP Modes[a] of Various $Zn[(RO)_2PS_2]_2$ Monomers from MSX

	R			
	Me	iBu	iPr	Phenyl
energy (kcal/mol)	567.2	541.0	562.2	536.8
$(Zn-DTP)_+$[b] (cm^{-1})	648	639	657	636
$(Zn-DTP)_-$[c] (cm^{-1})	502	496	506	493
$Zn-DTP_{ave}$	575	569	581	565

[a] Unscaled. [b] Antisymmetric combination of two symmetric stretch modes of the Zn−S bonds. [c] Symmetric combination of two symmetric stretch modes of the Zn−S bonds.

The predictions of the Zn−DTP modes and snap bond energies[24] are shown in Tables 7 and 8. These modes should be diagnostic for surface effects.

III.D. $Zn_2(DTP)_4$, the Dimer. *III.D.a. Structure.* It is well established[11,25,26] that in solution ZnDTPs exist as a chelated monomeric species in equilibrium with a dimeric form possessing a bridged structure. Indeed recent evidence indicates the presence of trimers, tetramers, and larger species.[31] There have not been previous characterizations of ZnDTP monomers and dimers either in the gas phase or in solution. However, the solid-state structures of $Zn\{[iPrO]_2PS_2\}_4$[27] and $Zn_2[(EtO)_2PS_2]_4$[28] have been reported. The former has a dimeric structure. Each zinc is chelated by one $[iPrO]_2PS_2$ ligand, and the two zinc atoms of the dimer unit are bridged by the other $[iPrO]_2PS_2$ groups. The latter exhibits a one-dimensional polymeric structure in which one $(EtO)_2PS_2$ ligand chelates each zinc atom, while the second ligand bridges zinc atoms in the chain.

There are various possible ways to build the $Zn_2[(MeO)_2PS_2]_4$ dimer (summarized in Table 9). Assuming first that all four DTP ligands have the *tt* conformation, we carried out *ab initio* calculations (HF/LAV3P***) with the following results.

(i) Since each Zn will have rough tetrahedral coordination of the four sulfurs, the most symmetric structure would have the bridging SPS and Zn in the plane and the terminal SPS groups perpendicular to this plane. This leads to D_{2h} symmetry.

(ii) The D_{2h} structure can be relaxed by allowing each PSP group to twist about its 2-fold axis. This removes the planes of symmetry, reducing the symmetry to D_2. We find that the energy drops by 23.84 kcal/mol. The driving force for this distortion is the SPS angle of the bridging DTP, which drops from 124° in D_{2h} to 117° in D_2 (the chelating DTP has 109° and isolated DTP^- has 119°).

(iii) Relaxing all symmetry requirements, we find that the structure with D_2 symmetry adjusts to C_2 symmetry and is stabilized by 3.6 kcal/mol. The origin of this D_2 to C_2 distortion is reduction of steric interactions between each bridging DTP and the chelating DTPs.

As the symmetry restrictions are relaxed in i, ii, and iii, the Zn···Zn distance decreases from 5.04 to 4.71 Å, indicating the ability of the dimer to adopt a more compact structure. We then considered allowing the conformation of the bridging DTPs to change.

(iv) Allowing the two bridging DTPs to adopt the g^+g^+ conformation retains the C_2 symmetry of the *tt* case in iii, but g^+g^+ leads to an energy 3.4 kcal/mol lower than for *tt*. This is because of further reduced steric interactions. In addition, the Zn···Zn distance decreases by 0.14−4.57 Å.

(v) Allowing the two bridging DTPs to adopt the tg^+ conformation leads to a structure with C_2 symmetry that is 6.2 kcal/mol lower in energy than for *tt*. This is the lowest energy

TABLE 9: Comparison of *ab Initio* Geometries[a] for the Dimer $Zn_2[(MeO)_2PS_2]_4$ from HF/LAV3P* Calculations**

ligands														
brid	chel	sym	energy (kcal/mol)	Zn−S		P−S		Zn−S−P		S−P−S	S−Zn−S	P−O		O−P−O	Zn···Zn
tt	*tt*	D_{2h}	33.63												
			chelating	2.482	2.482	2.027	2.027	83.8	83.8	109.0	83.3	1.587	1.587	97.5	5.042
			bridging	2.442	2.442	2.020	2.020	135.6	135.6	123.9	123.9	1.587	1.587	97.6	
		D_2	9.79												
			chelating	2.490	2.490	2.025	2.025	84.1	84.1	109.0	82.5	1.586	1.586	97.4	4.886
			bridging	2.437	2.437	2.027	2.027	112.9	112.9	117.4	121.8	1.585	1.585	98.0	
		C_2	6.15												
			chelating	2.502	2.507	2.026	2.026	84.2	84.1	109.1	82.5	1.588	1.588	97.5	4.710
			bridging	2.435	2.435	2.029	2.029	112.3	112.6	116.9	126.2	1.586	1.586	97.4	
g^+g^+	*tt*	C_2	2.76												
			chelating	2.494	2.495	2.024	2.024	83.8	83.8	109.4	82.9	1.590	1.590	97.2	
			bridging	2.447	2.443	2.015	2.016	105.5	105.6	118.4	123.0	1.597	1.597	105.9	4.573
tg^+	*tt*	C_2	0.0[b]												
			chelating	2.476	2.503	2.025	2.021	84.5	83.9	109.0	82.4	1.591	1.589	97.2	4.258
			bridging	2.449	2.446	2.027	2.015	103.7	101.6	115.2	121.0	1.594	1.586	102.3	

[a] Bond lengths in angstroms, and bond angles in degrees. [b] Total energy: −1148.078 60 hartrees.

TABLE 10: Comparison of Experimental, *ab Initio*, and FF Geometries[a] for the Dimer $Zn_2[(MeO)_2PS_2]_4$ with *tt* Chelating DTP and *tg* Bridging DTP

	Zn−S		P−S		Zn−S−P		S−P−S	S−Zn−S	P−O		O−P−O	Zn···Zn
expt[b]												
chelating	2.351	2.409	1.984	1.968	82.6	81.4	109.7	85.2	1.562	1.566	94.8	4.108
bridging	2.306	2.302	1.956	1.973	100.7	104.1	117.3	121.2	1.598	1.580	104.4	
QC[c]												
chelating	2.476	2.503	2.025	2.021	84.5	83.9	109.0	82.4	1.591	1.589	97.2	4.258
bridging	2.449	2.446	2.027	2.015	103.7	101.6	115.2	121.0	1.594	1.586	102.3	
MSX												
chelating	2.416[d]	2.415[d]	1.971	1.969	85.0	85.0	107.8	82.5	1.629	1.629	96.9	4.003
bridging	2.417[d]	2.461[d]	1.963	1.959	107.7	86.4	108.9	120.4	1.626	1.626	98.4	
UFF												
chelating	2.504	2.438	2.154	2.152	81.7	83.3	105.6	87.9	1.745	1.738	106.9	5.851
bridging	2.524	2.476	2.146	2.156	148.2	81.3	114.5	102.3	1.750	1.750	106.7	

[a] Bond lengths in angstroms, and bond angles in degrees. [b] Crystal structure of $Zn\{[iPrO]_2PS_2\}_4$.[27] [c] HF/LAV3P***. [d] The MSX FF was adjusted to reproduce the Zn−S bond distance expected from the best calculation [estimated to be 2.392A(MP2MSV****) = 2.463(HF/LAV3P***) − 0.071; see section III.D.d] rather than that of the HF/LAV3P*** level used for QC.

structure calculated for the dimer. The preference for bridging tg^+ ligands arises from the decreased steric effects in the dimer. Compared with structures having *tt* or g^+g^+ bridging DTPs, this structure bends along the C_2 symmetry axis. This results in a decreased Zn···Zn distance to 4.26 Å.

The solid-state structure of $Zn_2\{[iPrO]_2PS_2\}_4$ has the same C_2 conformation as our lowest energy structure. Comparisons between the structures from QC calculations on the dimer and crystal X-ray experiments are made in Table 10. Although there are obvious problems with the crystal structure (probably due to disorder of the alkyl groups) since some distances are quite unreasonable (e.g. one CC bond is 1.0 Å and a CO bond is 1.2 Å), it does agree with the theory for the O, P, and S regions, as indicated in Table 10.

The lowest energy structure of the dimer $Zn_2[(MeO)_2PS_2]_4$ from HF/LAV3P*** calculations is shown in Figure 7. Two of the four DTP groups have the *tt* conformation and function as *intra*chelating groups bound wholly to a single metal atom. The other two have the tg^+ conformation and function as bridging groups linking the two Zn(DTP) units together to form the dimer. The present *ab initio* calculations show that all phosphorus−sulfur bonds in the dimer are essentially *equivalent*. Thus the terminal DTPs have an average $PS_{chel} = 2.023$ Å (with a splitting of 0.004 Å due to steric effects), while the bridging DTPs have $PS_{brid} = 2.021$ Å (the splitting of 0.012 Å also due to steric effects). Thus the phosphorus−sulfur bond (average bond length of 2.022 Å) has character between that of single and double bonds. This agrees reasonably well with experiment, which has an average $PS_{chel} = 1.97$ Å with a splitting of 0.018 Å and an average $PS_{brid} = 1.965$ with a splitting of 0.017 Å.

A bigger discrepancy with experiment occurs for the ZnS distances. The calculations lead to $ZnS_{chel} = 2.490$ Å (splitting of 0.027 Å) and $ZnS_{brid} = 2.447$ Å (splitting of 0.003 Å). In contrast experiment leads to $ZnS_{chel} = 2.380$ Å (splitting of 0.058 Å) and $ZnS_{brid} = 2.304$ Å (splitting of 0.004 Å). The discrepancy of 0.110 Å for ZnS_{chel} and 0.143 Å for ZnS_{brid} is unusually large and will be addressed by additional calculations in section III.D.b below. We conclude that for ZnS_{chel} about 0.087 Å of the discrepancy is due to the level of the theory, leaving 0.023 Å that we attribute to packing effects (in the crystal).

The results from the MSX and UFF are also listed in Table 10. Those from the MSX are in good agreement with the QC results. In the MSX FF, we again used the formal charges of $Q_{Zn} = +2.0$ and $Q_{DTP} = -1$. The FF is the same as that for the $Zn(DTP)_2$ monomer except for the nonbonded S−S interaction parameters (eq 11), which were adjusted to reproduce the Zn···Zn distance from the *ab initio* structure of the $Zn_2(DTP)_4$ dimer.

III.D.b. Comparison to $Zn(F_2PS_2)_2$. As discussed above, the calculated ZnS bond lengths for the dimer deviate substantially from the crystal structure, with values 0.11 Å too long for ZnS_{chel} and 0.145 Å too long for ZnS_{brid}. This is an unexpectedly large discrepancy, and we carried out the following calculations on the model compound $Zn(F_2PS_2)_2$ to determine the origin. The results are summarized in Table 11 and Figure 8. We started with HF/LAV3P***, which led to $ZnS_{chel} = 2.490$ Å for $Zn_2(DTP)_4$ and $ZnS_{chel} = 2.481$ Å for $Zn(F_2PS_2)_2$, indicating that the model is suitable.

(i) To evaluate the effect of the effective core potential (ECP), we carried out all-electron calculations (HF/MSV***). We found a 0.022 Å decrease in the Zn−S bond length.

(ii) To evaluate the effect of f polarization functions on the zinc atom, we carried out all-electron calculations (HF/MSV****). We found a 0.001 Å decrease in the Zn−S bond length.

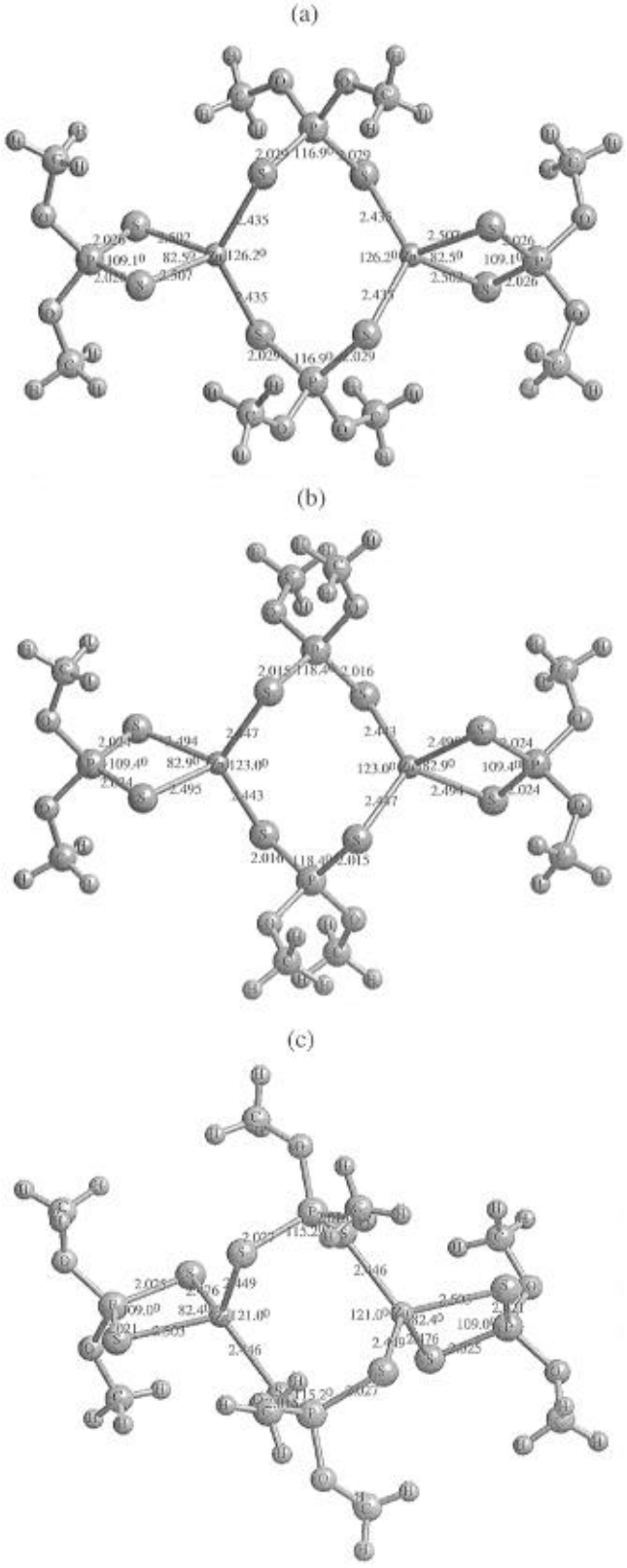

Figure 7. Structure of the $Zn_2(DTP)_4$ dimer from HF/LAV3P*** calculations. All three cases have the *tt* conformation of the chelating DTP, but the bridging DTPs are (a) *tt*, (b) g^+g^+, and (c) tg^+.

(iii) To evaluate the effect of electron correlation, we carried out Moller−Plesset theory (MP2/LAV3P***) calculations. This leads to a 0.048 Å decrease in the Zn−S bond length.

We also examined two other approaches to electron correlation. Generalized valence bond (GVB) theory (GVB/LAV3P***) leads to an increase of 0.016 Å. Such an increase is expected since only the Zn−S bond pairs are correlated, while MP2 is a

TABLE 11: Optimum Geometry of the Model Compound $Zn(F_2PS_2)_2$ as a Function of the Level of QC Calculation

	HF/LAV3P***[d]	HF/MSV***	HF/MSV****	MP2[c]/LAV3P***	MP2[c]/MSV****	DFT[a]/MSV***	GVB[b]/LAV3P**
				Bonds (Å)			
Zn−S	2.481	2.459	2.458	2.433	(2.410)[e]	2.456	2.497
S−P	1.989	1.990	1.990	1.997	(1.998)[e]	2.031	1.990
				Angles (deg)			
S−Zn−S	83.8	84.9	84.9	87.8	(88.9)[e]	88.1	83.4
S−P−S	112.9	113.1	113.0	115.3	(115.4)[e]	114.5	113.2

[a] The Becke gradient correction and the LYP correlation functional; see ref 13. [b] The Zn−S bond pairs are treated with GVB correlation. [c] All pairs. [d] Total energy −513.917 53 hartrees. [e] Estimated from other calculations.

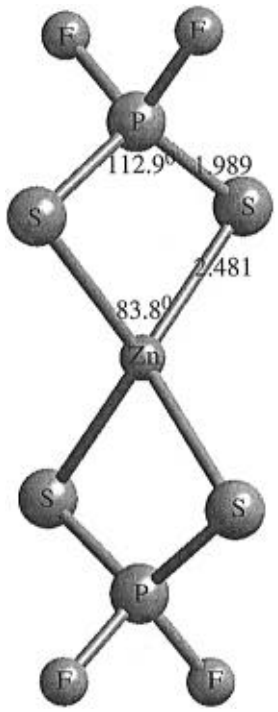

Figure 8. Structure of the model compound $Zn(F_2PS_2)_2$ from HF/LAV3P*** calculations.

more complete calculation. Density function theory (BLYP/MSV***) leads to a 0.025 Å decrease in the Zn−S bond length. We consider MP2 as more reliable.

Combining these various calculations we estimate that MP2/MSV**** would lead to a decrease of ZnS distances by 0.022 + 0.001 + 0.048 = 0.071 Å from the result for HF/LAV3P***. This leaves a discrepancy of 0.04 Å with experiment, which is still unexpectedly large.

As a second test, we carried out calculations on $ZnCl_2$, for which accurate gas phase experimental data[33] are available. We used a much larger basis set (including a triple-ζ contraction) and a more complete ECP (including only the 1s, 2s, and 2p core orbitals in the ECP) but not 3s and 3p. This is denoted as DOLG***. The results in Table 12 show that MP2/DOLG*** leads to a Zn−Cl bond distance 0.016 Å larger than experiment, which is an acceptable agreement with experiment.

Using the results from $ZnCl_2$, we estimate that the exact result for $Zn(F_2PS_2)$ is $ZnS_{chel} = 2.481 - 0.071 - 0.016 = 2.394$ Å. This suggests that the exact answer for gas phase $Zn_2(DTP)_4$ is ZnS = 2.490 − 0.087 = 2.403 Å. This is 0.023 Å larger than experiment, which we believe is attributable to packing effects in the crystal. Because of the strong ionic character in the Zn−S bond, polarization effects due to the dielectric medium of the crystal might also affect the length.

The experimental ZnS distances fall in the ranges of (i) 2.302−2.409 Å with an average of 2.342 Å for $\{Zn[(iPrO)_2PS_2]_2\}_2$,[27] (ii) 2.337−2.401 Å with an average of 2.359 Å for $\{Zn[(EtO)_2PS_2]_2\}_n$,[28] and (iii) 2.302−2.509 Å with an average of 2.375 Å for $\{Zn[(Et)_2PS_2]_2\}_2$.[34] These changes suggest that packing effects can modify the ZnS distance as much as 0.04 Å.

III.D.c. Vibrational Frequencies. Using the MSX FF, we calculated the vibrational frequencies of the dimer (Table 13). There are four PS_{anti} modes, two associated with the *tt* chelating DTPs and two from tg^+ bridging DTPs. As expected, the vibrational frequencies of the *tt* chelating DTPs of the dimer are similar to those of the *tt* DTPs of the monomer. Similar results are obtained for the symmetric stretch modes.

III.D.d. Energetics. The equilibrium concentration of monomer and dimer is dependent upon the nature of the alkyl group R on the DTP ligand, the nature of the solvent, and the ZnDTP conformation.[11,25,26]

From HF/LAV3P*** we calculated $\Delta E = -5.6$ kcal/mol for

$$2Zn[(MeO)_2PS_2]_2 \rightarrow Zn_2[(MeO)_2PS_2]_4 \qquad (12)$$

(that is, the dimer is more stable). The MSX FF leads to $\Delta E = -5.6$ kcal/mol, in excellent agreement. Using the calculated vibrational frequencies, we calculated the energies, enthalpy, and free energies of the dimerization process (12) as a function of temperature (Table 14). These results predict $\Delta G_{300K} = +9.3$ kcal/mol for R = Me and $\Delta G_{300K} = -3.0$ kcal/mol for R = iPr (both gas phase). The experimental value for R = iPr is $\Delta G_{300K} = -0.6$ kcal/mol (in CH_2Cl_2 solution), in reasonable agreement with theory. The difference between calculated and experimental results may be due to solvation effects.

IV. Summary

Structures, vibrations, and energetics of zinc dithiophosphates (ZnDTPs) have been studied by *ab initio* QC methods. Our results show that two phosphorus−sulfur bonds of the dithiophosphate for both ZnDTP monomers and dimers are *equivalent* and have characteristics between that of single and double bonds. The *ab initio* geometries agree well in the O, P, and S regions with those for the crystal structure of $Zn_2\{[iPrO]_2PS_2\}_4$.

Our results further show that the strong IR transition mode at about 650 cm^{-1} is the *antisymmetric stretch* of the phosphorus−sulfur bonds (not P═S), while the weaker transition mode at about 540 cm^{-1} is the *symmetric stretch* (not P−S). The

TABLE 12: Optimum Geometry of ZnH and $ZnCl_2$ for Various Levels of Calculation

	expt	HF/LAV3P***	MP2/LAV3P***	HF/DOLG***	MP2/DOLG***
ZnH	1.595[a]	1.635	(1.602)[e]	1.610[c]	1.577[c]
$ZnCl_2$	2.072[b]	2.142	(2.108)[e]	2.122[d]	2.088[d]

[a] Reference 32. [b] Reference 33. [c] The DOLG*** basis for Zn and the 6-31G** basis for H. [d] The DOLG*** basis for Zn and the LAV3P*** description of Cl (note that ClZnCl is linear). [e] Estimated from other calculations.

TABLE 13: Vibrational Frequencies (cm^{-1}) from MSX FF Calculations for the Phosphorus−Sulfur Bond Stretch Modes and for the Zn−DTP Modes

	$Zn_2[(MeO)_2PS_2]_4$ dimer		$Zn[(MeO)_2PS_2]_2$ monomer	
	chelating (*tt*)	bridging (tg^+)	($tt + tt$)	($tg^+ + tg^+$)
PS_{anti}[a]	645, 645	658, 659	646, 646	659, 660
PS_{sym}[b]	555, 555	577, 578	552, 552	570, 570
$(Zn-DTP)_+$[b]	567	562		
$(Zn-DTP)_-$[b]	504	516		

[a] Scaling factors of 0.937 for PS_{anti} and 1.01 for PS_{sym} were used. [b] Unscaled.

TABLE 14: Energetics, Enthalpy, and Free Energies (kcal/mol) of the Dimerization Process (12) as a Function of Temperature from MSX FF

R	ΔE_{0K}	ΔH_{0K}	ΔH_{300K}	ΔG_{300}	ΔG_{300}^{exp} [25]
Me	−5.6[b]	−5.6	−5.3	+9.3	
iPr	−21.8	−21.8	−21.7	−3.0	−0.6

[a] In chloroform. [b] HF calculations give −5.6.

two vibrational frequencies for each of these DTP modes in $Zn[(MeO)_2PS_2]_2$ result from the modes of isolated DTP splitting into sum and difference modes by zinc-induced coupling of degenerate local modes. Thus the theory replaces the P═S, P−S paradigm with a resonance sesquibond order description much as for RCO_2^-.

Ab initio results were used to develop the MSX FFs, which produce accurate structures, vibrational frequencies, and energetics for DTP systems. Thus the MSX FF should be useful in simulating the structures, vibrations, and energetics of DTPs on metal and metal oxide surfaces.

Acknowledgment. This research was supported by the Chevron Chemical Co. (Oronite Technology Group), by the DOE-BCTR, and by NSF GCAG (ASC 92-100368). The facilities of the MSC are also supported by grants from Chevron Petroleum Technology Co., Asahi Chemical, Aramco, Asahi Glass, BP Chemical, Hercules, Xerox, Hughes Research Lab., Chevron Research and Technology Co., and Beckman Institute. Part of the calculations were carried out at the San Diego Supercomputer Center, the Pittsburgh Supercomputer Center, and National Center for Supercomputer Applications, and the JPL Supercomputer Center.

Supporting Information Available: Figure 1S and Tables 1S−3S (5 pages). Ordering information is given on any current masthead page.

References and Notes

(1) McGeehan, J. A.; Graham, J. P.; Yamaguchi, E. S. SAE 902162; SAE: Warrendale, PA, 1990.

(2) Roby, S. H. *Lubr. Eng.* **1991**, *47*, 413. Benchaita, M. T. *Lubr. Eng.* **1991**, *47*, 893.

(3) Born, M.; Hipeaux, J. C.; Marchand, P.; Parc, G. In *Engine Oils and Automotive Lubrication*; Bartz, W. J., Ed.; Marcel Dekker: New York, 1993; pp 335−358.

(4) Yamaguchi, E. S.; Ryason, P. R. *Proceedings of the Fourth International Symposium on the Performance Evaluation of Automotive Fuels and Lubricants*; Birmingham, U.K., CEC, 1, 1993. Wooton, D. L.; Hughes, D. W. *Lubr. Eng.* **1987**, *43*, 736. Willermet, P. A.; Pieprzak, J. M.; Dailey, D. P.; Carter, R. O.; Lindsay, N. E., III; Haack, L. P.; deVries, J. E. *J. Tribol.* **1991**, *113*, 38.

(5) Roby, S. H.; Supp, J. A. SAE 952342; SAE: Warrendale, PA, 1995.

(6) Korcek, S. Tribology 2000: 8th Intl. Coll., Bartz, W. J., Ed.; Technische Akademic Esslingen: Octfildem, 1992; pp 11.1-1−11.1-6.

(7) Caracciolo, F.; Spearot, J. A. SAE 760562; SAE: Warrendale, PA, 1976. Spearot, J. A.; Caracciolo, F. SAE 770637; SAE: Warrendale, PA, 1977. Minamitani, H.; Ikuyama, A.; Machida, C.; Kawashima, K.; Matsudaira, Y.; Furui, J. *J. Jpn. Petrol. Inst.* **1978**, *21*, 116. Wiliamson, W. B.; Perry, J.; Gross, R. L.; Gandhi, H. S.; Beason, R. E. SAE 841406; SAE: Warrendale, PA, 1984. Chamberline, W. B.; Zalar, F. V. SAE 841407; SAE: Warrendale, PA, 1984. Williamson, W. B. SAE 852097; SAE: Warrendale, PA, 1989. Brett, P. S.; Neville, A. L.; Preston, W. H.; Williamson, J. SAE 890490; SAE: Warrendale, PA, 1989. Joy, G. C. SAE 852099; SAE: Warrendale, PA, 1989. Niura, Y. SAE 852220; SAE: Warrendale, PA, 1989.

(8) Hayashi, S.; Stonebraker, C. M.; Cisson, C. M.; Rausina, G. A. *Toraiborojisuto* **1995**, *40*, 286.

(9) Dickert, J. J., Jr.; Rowe, C. N. *J. Org. Chem.* **1967**, *37*, 647. Ford, J. F. *J. Inst. Pet.* **1968**, *54*, 198. Jones, R. B.; Coy, R. C. *ASLE Trans.* **1980**, *24*, 91. Benfaremo, N.; Liu, C. S. *Lubrication* **1990**, *76*, 1. Liston, T. V. *Lubr. Eng.* **1992**, *48*, 389.

(10) (a) Gallopoulos, N. E. *Prepr.−Div. Pet. Chem., Am. Chem. Soc.* **1966**, *11*, 3. (b) Zimina, K. I.; Kotova, G. G.; Sanin, P. I.; Sher, V. V.; Kuzmina, G. N. *Neftekhimiya* **1965**, *5*, 629. (c) Rockett, J. *Appl. Spectrosc.* **1962**, *16*, 39. (d) Yamaguchi, E. S.; Ryason, P. R. *Tribol. Trans.* **1993**, *36*, 367. (e) Yamaguchi, E. S.; Ryason, P. R.; Labrador, E. Q. *Tribol. Trans.* **1995**, *38*, 243.

(11) Harrison, P. G.; Sebald, A. *J. Chem. Res., Synop.* **1991**, 340; *J. Chem. Res., Miniprint* **1991**, 3116.

(12) Greeley, B. H.; Russo, T. V.; Mainz, D. T.; Friesner, R. A.; Langlois, J.-M.; Goddard, W. A.; Donnelly, R. E., III; Ringnalda, M. N. *J. Chem. Phys.* **1994**, *101*, 4028.

(13) Ringnalda, M. N.; Langlois, J.-M.; Greeley, B. H.; Murphy, R. B.; Russo, T. V.; Cortis, C.; Muller, R. P.; Marten, B.; Donnelly, R. E., Jr.; Mainz, D. T.; Wright, J. R.; Pollard, W. T.; Cao, Y.; Won, Y.; Miller, G. H.; Goddard, W. A., III; Friesner, R. A. *PS-GVB v2.24*; Schrödinger Inc.: Portland, OR, 1995.

(14) Hay, P. J.; Wadt, W. R. *J. Chem. Phys.* **1985**, *82*, 270; *Ibid.* **1985**, *82*, 284; *Ibid.* **1985**, *82*, 299. See also: Melius, C. F.; Goddard, W. A., III *Phys. Rev. A* **1974**, *10*, 1528.

(15) Frisch, M. J.; Pople, J. A.; Binkley, J. S. *J. Chem. Phys.* **1984**, *80*, 3265.

(16) Rappé, A. K.; Goddard, W. A., III. Unpublished. This basis is denoted as MSV in ref 13.

(17) Frisch, M. J.; Trucks, G. W.; Schlegel, H. B.; Gill, P. M. W.; Johnson, B. G.; Wong, M. W.; Foresman, J. B.; Robb, M. A.; Head-Gordon, M.; Replogle, E. S.; Gomperts, R.; Andres, J. L.; Raghavachari, K.; Binkley, J. S.; Gonzalez, C.; Martin, R. L.; Fox, D. J.; Defrees, D. J.; Baker, J.; Stewart, J. J. P.; Pople, J. A. *Gaussian 92*; Gaussian, Inc.: Pittsburgh, PA, 1993.

(18) Dolg, M.; Wedig, U.; Stoll, H.; Preuss, H. *J. Chem. Phys.* **1987**, *86*, 866.

(19) Chirlian, L. E.; Francl, M. M. *J. Comput. Chem.* **1987**, *8*, 894. Woods, R. J.; Khalil, M.; Pell, W.; Moffat, S. H.; Smith, V. H., Jr. *J. Comput. Chem.* **1990**, *11*, 297. Breneman, C. M.; Wiberg, K. B. *J. Comput. Chem.* **1990**, *11*, 361.

(20) (a) Mayo, S. L.; Olafson, B. D.; Goddard, W. A., III *J. Phys. Chem.* **1990**, *94*, 8897. (b) Rappé, A. K.; Casewit, C. J.; Colwell, K. S.; Goddard, W. A., III; Skiff, W. M. *J. Am. Chem. Soc.* **1992**, *114*, 10025.

(21) Dasgupta, S.; Goddard, W. A., III *J. Chem. Phys.* **1989**, *90*, 7207. Yamasaki, T. E.; Dasgupta, S.; Goddard, W. A., III *J. Chem. Phys.*, in press.

(22) *BIOGRAF/POLYGRAF*; V 3.21 (Caltech Version V 3.30); Molecular Simulations Inc.: San Diego, CA.

(23) Rappé, A. K.; Goddard, W. A., III *J. Phys. Chem.* **1991**, *95*, 3358.

(24) The snap bond energy for A−B is obtained by fixing the internal coordinates of A and of B and then separating the fragments to infinity.

(25) Harrison, P. G.; Brown, P.; Hynes, M. J.; Kiely, J. M.; McManus, J. *J. Chem. Res., Miniprints* **1991**, 1636; *J. Chem. Res., Synop.* **1991**, 174.

(26) Harrison, P. G.; Kikabhai, T. *J. Chem. Soc. Dalton Trans.* **1987**, *4*, 807. Harrison, P. G.; Brown, P.; McManus, J. *Inorg. Chim. Acta* **1992**, *202*, 3.

(27) Lawton, S. L.; Kokotailo, G. T. *Inorg. Chem.* **1969**, *8*, 2410.

(28) Ito, T.; Igarashi, T.; Hagihara, H. *Acta Crystallogr. Sect. B* **1969**, *25*, 2303.

(29) Pauling, L. *The Nature of the Chemical Bond*; Cornell University Press: Ithaca, NY, 1960.

(30) Harrison, P. G.; Begley, M. J.; Kikabhai, T.; Killer, F. *J. Chem. Soc., Dalton Trans.* **1986**, *5*, 929.

(31) Yamaguchi, E. S.; Primer, R. L.; Aragon, S. R.; Labrador, E. Q. *Tribol. Trans.*, accepted for publication.

(32) *CRC Handbook of Chemistry and Physics*, 74th ed.; CRC Press: Boca Raton, FL, 1993; p 9−23.

(33) Hargittai, M.; Tremmel, J.; Hargittai, I. *Inorg. Chem.* **1986**, *25*, 3164.

(34) Calligaris, M.; Nardin, G.; Ripamonti, A. *J. Chem. Soc. A* **1970**, 714.

JP960649J